Available online at www.sciencedirect.com

ScienceDirect

Procedia Structural Integrity 64 (2024) 1500–1507

Structural Integrity Procedia

www.elsevier.com/locate/procedia

SMAR 2024 – 7th International Conference on Smart Monitoring, Assessment and Rehabilitation of Civil Structures

Experimental and theoretical study on flexural behavior of hybrid bonded CFRP RC beams

A. Codina[a]*, C. Barris[a], M. Baena[a], T. D'Antino[b], L. Torres[a]

[a]*AMADE, University of Girona, C/ Universitat de Girona 4 (Campus Montilivi), 17003 Girona, Spain*
[b]*Politecnico di Milano, Department of Architecture, Built Environment and Construction Engineering, Piazza Leonardo da Vinci 32, 20133 Milan, Italy*

Abstract

Fiber reinforced polymer (FRP) composites are widely used to strengthen reinforced concrete (RC) structures due to their high mechanical and durability properties compared to traditional materials. However, intermediate crack debonding (ICD) failure limits the effectiveness of strengthening RC beams in flexure with externally bonded (EB)-FRP laminates. Anchorage of the FRP can mitigate this debonding, enhancing the efficiency of FRP strengthening. Hybrid bonding (HB)-FRP emerged as a viable method for delaying/preventing debonding of EB-FRP RC beams. HB combines adhesive bonding from EB with mechanical fastening through metallic plates, increasing resistance to debonding. While previous research explored the bonding capacity of the HB connection using FRP sheets in single-shear tests, few simplified approaches exist for predicting the bending capacity of strengthened beams. In this paper, the feasibility of HB systems to delay ICD of RC flexural elements strengthened with carbon FRP (CFRP) pre-cured laminates is assessed through experimental and theoretical studies. For this purpose, three RC beams strengthened with CFRP are tested, one using EB and two using HB with different anchor spacings. Results include load-deflection response, flexural capacity and failure mode. Experimental results are compared to literature provisions. Results show that the HB technique consistently improves the flexural performance of the beam in all considered cases.

Keywords: Reinforced concrete; externally bonded reinforcement, hybrid bonded reinforcement, anchors, debonding.

* Alba Codina
E-mail address: alba.codina@udg.edu

10.1016/j.prostr.2024.09.401

1. Introduction

In recent years, there has been a growing acceptance of the use of fiber reinforced polymers (FRP) for reinforcing concrete structures due to their inherent advantages over traditional materials. The externally bonded (EB) reinforcement technique is widely employed to enhance the structural performance of reinforced concrete (RC) elements in various loading scenarios and was proven to be effective in improving the bending, shear, torsion, and axial capacities (Bakis et al., 2002). However, a common challenge observed in existing literature is the occurrence of intermediate crack debonding (ICD), primarily observed in flexural applications (Mazzotti et al., 2016), which significantly limits the effective exploitation of FRP properties.

To address the issue of ICD, current design guidelines (ACI Committee 440, 2017; Consiglio Nazionale delle Ricerche (CNR), 2013; fib Task Group 5.1, 2019) have proposed several analytical models with different levels of approximation. These models can accurately predict ICD failure but are sensitive to parameters such as the fracture energy of the interface, thereby necessitating careful calibration against experimental data (Codina et al., 2023). Additionally, researchers have explored various anchorage methods, including mechanically fastened (MF) metallic anchors and hybrid configurations like the hybrid bonded (HB)-FRP system, which combines MF and EB techniques to enhance resistance against debonding (Chen et al., 2018; Wu & Huang, 2008).

Efforts have been directed towards developing methods to predict the bonding capacity of HB joints, considering factors such as bonded length, number of anchors, and pressure exerted by the fasteners. Analytical and numerical models (Chen et al., 2018; Gao et al., 2019; X. H. Gao et al., 2023; Wu & Liu, 2013; Zhang et al., 2022) have been proposed to estimate bonding capacity, with some studies achieving good correlation between experimental data and numerical simulations. However, existing design methods derived from single-shear test configurations may not accurately predict ICD in RC beams due to the different stress configuration at both ends of the FRP between flexural cracks.

Few models have been developed to predict the flexural behavior of HB-FRP strengthened RC beams, including analytical, finite element method (FEM), and simplified bond strength models (Chen et al., 2019; Gao et al., 2023; Zhang et al., 2021, 2021, 2023). While analytical models offer descriptive insights, they lack flexibility in implementing different bond-slip laws, which are essential for HB systems. In contrast, FEM models allow for the introduction of several bond-slip laws but may be complex for designing applications. Simplified bond strength models provide a concise approach but rely on empirical coefficients calibrated with limited experimental data.

In this study, a detailed description of the different models found in the literature to predict the flexural capacity of HB-FRP strengthened RC beams is presented along with an experimental campaign including RC beams strengthened with EB and HB-carbon FRP (CFRP) precured laminates. Experimental results are presented and discussed in terms of modes of failure, flexural capacity, load-displacement response, and load-strain response in the CFRP. The experimental flexural capacity is compared with the described prediction models.

2. Theoretical models

Few simplified models have been proposed to predict the flexural capacity of HB-FRP strengthened RC beams (Chen et al., 2019; Gao et al., 2023; Zhang et al., 2021). The analytical models considered in this paper share a common framework to evaluate the maximum tensile force in the FRP laminate (P_f) involving two integral components (as per Eq. (1)): the adhesive strength of the EB FRP (P_{EB}), which is computed using established equations from existing literature, and the frictional strength of the anchors (P_{HB}). The anchor contribution is calculated by Eq. (2), where n represents the number of anchors within the shear-span of the beam, u is the frictional coefficient between two rough concrete surfaces, and N_a denotes the pressure applied onto the FRP strip by a single anchor. The values of the parameters used by the literature models are reported in Table 1 (Eqs. (3)-(13)).

$$P_f = P_{EB} + P_{HB} \leq \varepsilon_{fu} E_f A_f \tag{1}$$

$$P_{HB} = nuN_a \tag{2}$$

Table 1. Prediction models for ICD considered in this paper.

Reference	Strength model	Eq.
Chen et al. (2019)	Adhesive strength P_{EB} (analytical model from Chen et al. (2018))	
	$P_{EB} = \frac{b_f \cdot \tau_{f1}}{\lambda_1}$	(3)
	where	
	$\lambda_1 = \sqrt{\left(\frac{1}{E_c \cdot A_c} + \frac{1}{E_f \cdot A_f}\right)\frac{b_f \cdot \tau_{f1}}{s_1}}$	(4)
	Frictional strength P_{HB} (analytical model from Chen et al. (2018))	
	$P_{HB} = nuN_a$	
	u = 0.96 (from Wu et al. (2010))	
	$N_a = \frac{M_t}{k}$	(5)
	where	
	M_t = torque applied to one bolt	
	k = twisting coefficient calibrated to be 0.001264 m	
Zhang et al. (2021)	Adhesive strength P_{EB} (Teng et al. (2003))	
	$P_{EB} = \alpha \cdot b_f \cdot t_f \cdot k_b \cdot \beta_l \sqrt{\frac{E_f\sqrt{f_{cm}}}{t_f}}$	(6)
	where	
	α = 0.48 or 0.94 for EB, and 0.48 for HB [1]	
	$k_b = \sqrt{\frac{2 - b_f/b}{1 + b_f/b}} \geq 1$	(7)
	$\beta_l = \begin{cases} sin\frac{\pi l_b}{2l_e} & \text{for } l_b \leq l_e \\ 1 & \text{for } l_b > l_e \end{cases}$	(8)
	$l_e = \sqrt{\frac{E_f \cdot t_f}{\sqrt{f_{cm}}}}$	(9)
	Frictional strength P_{HB} (from Gao (2020))	
	$P_{HB} = nuN_a$	
	u = 0.96 (from Wu et al. (2010))	
	$N_a = \frac{2M_t}{k_l \cdot d_l}$	(10)
	where	
	k_l = twisting coefficient calibrated to be 0.218	
	d_l = fastener diameter	
Gao et al. (2023)	Adhesive strength P_{EB} (Modifying the model from Teng et al. (2003) to include the effect of the anchor spacing, denoted as S_a)	
	$P_{EB} = S_a \cdot \alpha \cdot b_f \cdot t_f \cdot k_b \cdot \beta_l \sqrt{\frac{E_f\sqrt{f_{cm}}}{t_f}} + 410$	(11)
	where	
	α = 0.48 or 0.94 for EB, and 0.48 for HB [1]	
	$S_a = \begin{cases} 1 & if\ S_{anc} \geq l_e \\ \frac{l_e}{S_{anc}} & if\ S_{anc} < l_e \end{cases}$	(12)
	Frictional strength P_{HB} (from Gao (2020))	

$P_{HB} = nuN_a$

u = 0.96 (from Wu et al. (2010))

$$N_a = \frac{M_t}{k} \quad (13)$$

where

M_t = torque applied to one bolt

k = twisting coefficient calibrated to be 0.001264 m

[1] Teng et al. (2003) suggest a design value of α = 0.48, while reporting a mean value of α = 0.94 for predicting ICD in EB FRP-strengthened RC beams.

3. Experimental program

Three RC beams were tested under a 4-point bending configuration with a shear span of 900 mm to induce failure by ICD, as suggested by (Al-Saawani et al., 2020). The specimens were externally reinforced with one CFRP strip with width 50 mm × thickness 1.4 mm ($b_f \times t_f$). Dimensions are illustrated in Fig. 1, showing a span length of 2200 mm and a cross section with 140 mm width and 180 mm depth. The internal tensile steel reinforcement consisted of two bars of diameter 10 mm as tensile reinforcement, two bars of diameter 6 mm as compression reinforcement, and stirrups of diameter 8 mm placed along the beam length with a spacing of 100 mm to avoid shear failure. The specimens were designated as X-SY, where X is the strengthening technique (EB or HB) and Y is the anchor spacing in mm, when present (100 mm or 300 mm). The main parameters of the program were the strengthening technique (EB and HB) and the anchor spacing.

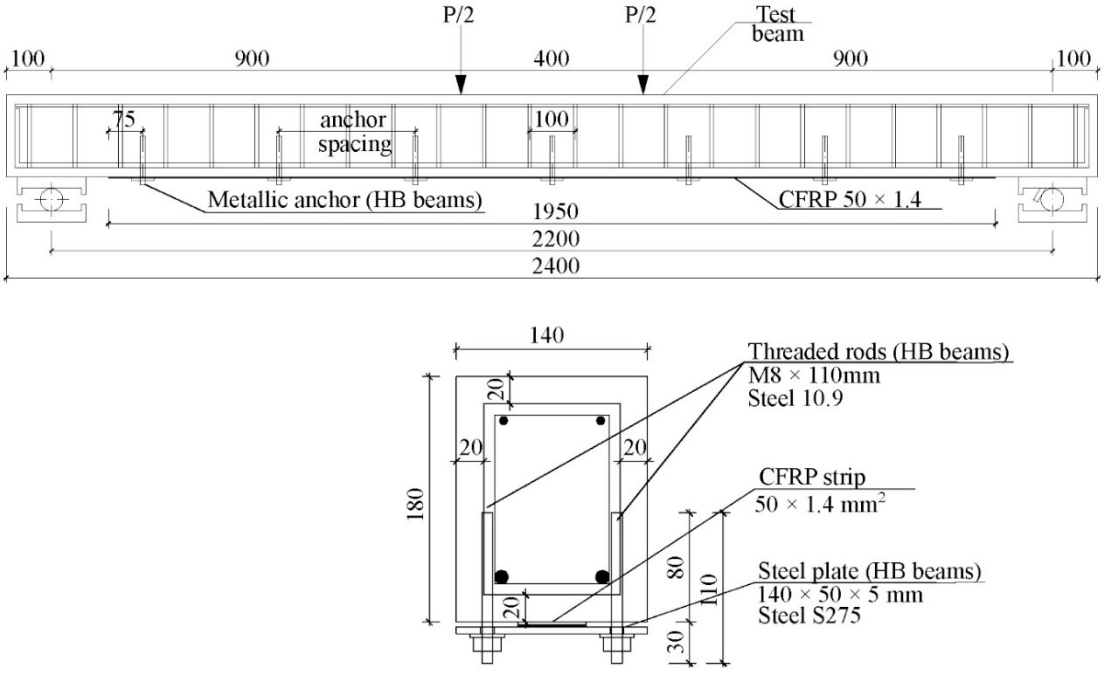

Fig. 1. Beam specimens (dimensions in mm).

The experimental compressive strength (f_{cm}), tensile strength (f_{ctm}), and modulus of elasticity (E_c) of the concrete were determined following the protocols in UNE-EN 12390-3 (2011), UNE-EN 12390-6 (2010), and ASTM C469/C469M-10 (2010) standards. The results obtained were 45.98 MPa (with a Coefficient of Variation,

CoV=5.59%) for cylinder compressive strength, 3.94 MPa (CoV=2.93%) for tensile strength, and 36.21 GPa (CoV=0.60%) for modulus of elasticity.

The mechanical properties of the steel used for internal reinforcement were determined from tensile tests according to UNE-EN ISO 15630-1 (2011). The average yielding strength (f_y), yielding strain (ε_y), and modulus of elasticity (E_s) were found to be 569.96 MPa (CoV=2.18%), 0.27% (CoV=0.76%), and 208.58 GPa (CoV=1.80%), respectively.

The mechanical properties of the unidirectional CFRP pultruded laminates provided by the manufacturer (S&P C-Laminate) include a tensile strength (f_{fu}) of 2800 MPa, a tensile strain (ε_{fu}) of 1.6%, and a modulus of elasticity (E_f) of 170 GPa.

The two-component epoxy resin used to bond the CFRP laminates was a thixotropic and solvent-free adhesive, with a density of approximately $1.6 \cdot 10^3$ kg/m^3. According to the manufacturer (S&P Resin 220 HP) data sheet, the minimum values of the tensile strength and modulus of elasticity of this epoxy resin after a curing time of 7 days are 15 MPa and 7.10 GPa, respectively.

Surface preparation for the EB technique involved removing the outer layer of concrete through bush-hammering (Iovinella et al., 2013). After that, in the specimens strengthened using the HB technique, 10 mm diameter holes were drilled into the concrete to a depth of 80 mm, cleaned with compressed air, filled with a polyester hybrid mortar, and then threaded rods were inserted. Both techniques involved bonding the CFRP laminate onto the concrete surface, previously cleaned with compressed air, applying a thin layer of epoxy resin. After 24 hours of curing the epoxy resin, S275 structural steel plates of dimensions 140 × 50 × 5 mm were bonded onto CFRP laminates in the HB specimens using the same epoxy resin. Washers and nuts were fastened with a torque of 10 Nm one day after bonding the steel plates. The strengthening system was cured for 11 days at laboratory conditions before testing.

4. Experimental results and discussion

Table 2 presents the recorded applied load, midspan deflection, and FRP strain values at cracking (P_{cr}, δ_{cr}, $\varepsilon_{f,cr}$), yielding (P_y, δ_y, $\varepsilon_{f,y}$), and failure (P_{max}, δ_{max}, $\varepsilon_{f,max}$), along with the failure mode for each beam. The bending capacity increased ($\Delta P_{max,EB}$) in HB specimens compared to EB without significantly affecting the load, deflection, and strain values at cracking and yielding. With an anchor spacing of 300 mm, there was a delay in the ICD failure mode, resulting in an 8% enhancement in load-carrying capacity. Nevertheless, reducing the anchor spacing to 100 mm completely prevented debonding, causing failure by concrete crushing (CC) at the midspan top section and leading to a 27% increase in maximum load compared to the EB. Moreover, HB technique led to a more efficient use of the CFRP laminate, which could attain higher strain values with respect to those of the EB technique, increasing from approximately 0.63% to 0.74% in specimen HB-S300 and to 1.23% in specimen HB-S100.

Table 2. Experimental results of beam tests

Specimen label	Cracking			Yielding			Failure (peak load)					
	P_{cr} (kN)	δ_{cr} (mm)	$\varepsilon_{f,cr}$ (%)	P_y (kN)	δ_y (mm)	$\varepsilon_{f,y}$ (%)	P_{max} (kN)	δ_{max} (mm)	$\varepsilon_{f,max}$ (%)	$\Delta P_{max,EB}$ (%)	$\Delta\varepsilon_{f,max,EB}$ (%)	Failure mode
EB	9.86	1.54	0.02	43.73	16.92	0.42	53.23	24.36	0.63	-	-	ICD
HB-S300	9.69	1.49	0.03	43.07	15.04	0.41	57.68	58.57	0.74	8	17	ICD
HB-S100	9.72	1.64	0.03	44.29	15.94	0.43	67.77	44.54	1.23	27	95	CC

Regarding the failure modes, in the EB specimen, the laminate suffered ICD, detaching from the surface along with the weak outer layer of concrete, as expected. While precisely identifying the exact initiation point of debonding is challenging, the widest and deepest cracks were observed at considerable distances from the end anchorage region and near the load application locations. From visual inspection of the specimen HB-S300, it was observed that the laminate only detached in specific areas near the load application points, as illustrated in Fig. 2a. The anchors effectively retained the remaining portion of the laminate attached to the surface. However, the test experienced a sudden significant decrease in load capacity after the peak load due to the debonding of the FRP laminate, which the beam was not able to recover. In the case of specimen HB-S100, also localized debonding could be observed.

Nevertheless, anchors succeeded in maintaining the laminate attached to the beam until failure by CC occurred (Fig. 2b).

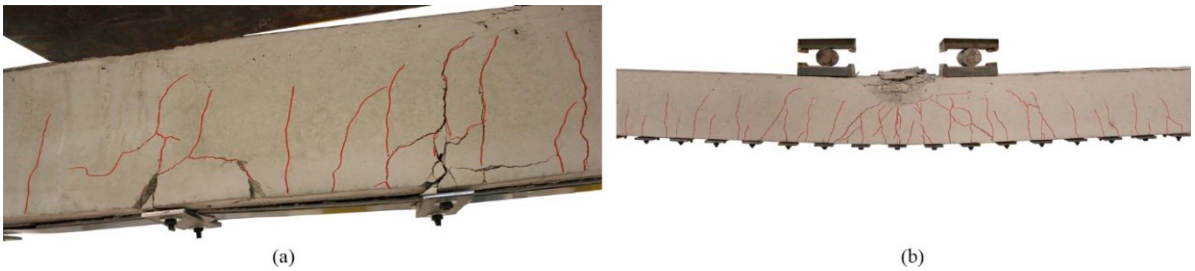

Fig. 2. (a) ICD in beam HB-S300; (b) CC in beam HB-S100.

5. Comparison with prediction models from the literature

The predicted load capacity, failure mode and ratio of theoretical to experimental maximum load applied to the beam ($P_{max,th}$ /$P_{max,exp}$) for each prediction model are reported in Table 3. Calculations for EB tested beam were performed using both design and mean values of α (0.48 and 0.94, respectively). However, for HB specimens, since the models are calibrated with α = 0.48, only this value was used in the calculations. The model proposed by Chen et al. (2019) provided a conservative value for the EB specimen, exhibiting a ratio of 0.34. However, the predicted anchor contribution significantly increased the load capacity of the HB specimens, resulting in more accurate predictions for anchored beams with ratios of 0.85 and 0.92 for the anchor spacings of 300 mm and 100 mm, respectively.

Table 3. Comparison between predicted and experimental load capacities.

Specimens	α	Experimental		Chen et al. (2019)			Zhang et al. (2021)			Gao et al. (2023)		
		$P_{max,th}$ (kN)	Failure mode	$P_{max,th}$ (kN)	Failure mode	$P_{max,th}$ /$P_{max,exp}$	$P_{max,th}$ (kN)	Failure mode	$P_{max,th}$ /$P_{max,exp}$	$P_{max,th}$ (kN)	Failure mode	$P_{max,th}$ /$P_{max,exp}$
EB	0.94	53.23	ICD	18.24	ICD	0.34	50.45	ICD	0.95	50.45	ICD	0.95
	0.48	53.23	ICD	18.24	ICD	0.34	33.67	ICD	0.63	33.67	ICD	0.63
HB-S300	0.48	57.68	ICD	49.19	ICD	0.85	50.79	ICD	0.88	54.21	ICD	0.94
HB-S100	0.48	67.77	CC	62.68	ICD	0.92	69.79	CC	1.03	69.79	CC	1.03

On the other hand, the models proposed by Zhang et al. (2021) and Gao et al. (2023), using the same formulation for EB, provided an accurate prediction for the EB specimen, displaying a ratio of 0.95 when using α = 0.94. However, when using α = 0.48, results become more conservative, with a ratio of 0.63. This difference can be attributed to the mean value reported by Teng et al. (2003) of 0.94 in contrast with the design value of 0.48.

Regarding the predictions for the HB beam with an anchor spacing of 300 mm, the model of Zhang et al. (2021) yielded a conservative ratio of 0.88. Comparing the predicted ultimate load (50.79 kN) to the EB prediction for α = 0.48 (33.67 kN), a 51% increase was observed, while only a 1% increase was obtained when compared to the EB prediction for α = 0.94 (50.45 kN). In contrast, the experimental increase in load capacity of HB-S300 with respect to EB was equal to 8% ($\Delta P_{max,EB}$ in Table 2). This highlights the need for more tests to recalibrate the model if an α = 0.48 is considered. On the other hand, the model of Gao et al. (2023) provided more accurate results for the beam HB-S300, with a ratio of 0.94, experiencing a higher increase in load capacity compared to the EB specimen than in the model of Zhang et al. (2021). This difference may be related to the calibration of this model, which takes into account the anchor spacing.

For the beam with an anchor spacing of 100 mm, the predicted failure mode is CC for both Zhang et al. (2021) and Gao et al. (2023) models, the same as the experimental one, showing a ratio of 1.03. Further experimental tests should be designed and performed to achieve debonding failure modes when using a high number of anchors, to improve the model reliability and theoretical results accuracy.

6. Conclusions

In this paper, an analysis of different models from the literature for predicting the flexural capacity of HB-FRP strengthened RC beams was conducted, and their outcomes were compared with experimental results from a campaign comprising three RC beams reinforced with CFRP laminates using EB and HB techniques, with two anchor spacings for the HB method. From this study, the following conclusions can be drawn:

- HB enhanced the flexural capacity of the EB specimens by providing a residual strength after debonding of the FRP laminate, with an 8% increase in specimen HB-S300 and a 27% in HB-S100. Additionally, the HB technique led to a more efficient use of the CFRP laminate, yielding higher strain values, with increases up to 17% in HB-S300 and 95% in HB-S100.
- The reduction in anchor spacing from 300 mm to 100 mm effectively localized debonding, allowing the load to increase until failure due to concrete crushing, while in EB and HB-S300 beams failure was attributed to ICD.
- A comparison with existing applicable models from the literature highlighted the absence of general formulations that accurately predict the load-carrying capacity for both EB and HB techniques. These models tended to underestimate the capacity of EB, requiring a compensatory high contribution from the anchor to achieve accurate results in HB specimens. Developing strength models on a combination of EB and HB contributions require accuracy in predicting the load capacity of the EB specimens. Based on results of the comparative analysis, a coefficient $\alpha = 0.94$ for mean values is suggested for the models Zhang et al. (2021) and Gao et al. (2023) instead of $\alpha = 0.48$, which was originally intended for design purposes. The formulation for the anchor contribution should be recalibrated for this new value.
- The model of Gao et al. (2023), which includes the effect of the anchor spacing, yielded the most accurate predictions, highlighting the importance of investigating the main parameters of the anchorage system. Future studies should include the effect of the pre-tightening force applied to the bolts in the load-carrying capacity of the system without having to calibrate the model for every application, as well as the effect of the anchor geometry and material parameters.

Acknowledgements

The authors wish to acknowledge the support of S&P Clever Reinforcement Ibérica Lda. for supplying the laminates and the epoxy resin used in this study.

This work was supported by the Spanish Ministry of Science and Innovation (MICIU/ AEI) under project PID2020-119015GB-C22 (MICIU/AEI/10.13039/5011000011033) and the Generalitat de Catalunya, under the Grant number 2020_FISDU 00476.

References

ACI Committee 440. (2017). ACI 440.2R-17: Guide for the design and construction of externally bonded FRP systems for strengthening concrete structures. American Concrete Institute (ACI).

Al-Saawani, M. A., El-Sayed, A. K., & Al-Negheimish, A. I. (2020). Effect of shear-span/depth ratio on debonding failures of FRP-strengthened RC beams. Journal of Building Engineering, 32, 101771. https://doi.org/10.1016/J.JOBE.2020.101771

ASTM C469/C469M-10. (2010). Standard Test Method for Static Modulus of Elasticity and Poisson's Ratio of Concrete in Compression.

Bakis, C. E., Bank, L. C., Asce, F., Brown, V. L., Asce, M., Cosenza, E., Davalos, J. F., Asce, A. M., Lesko, J. J., Machida, A., Rizkalla, S. H., & Triantafillou, T. C. (2002). Fiber-Reinforced Polymer Composites for Construction-State-of-the-Art Review. Journal of Composites for Construction, 6(2), 73–87. https://doi.org/10.1061/ASCE1090-026820026:273

Chen, C., Sui, L., Xing, F., Li, D., Zhou, Y., & Li, P. (2018). Predicting bond behavior of HB FRP strengthened concrete structures subjected to different confining effects. Composite Structures, 187, 212–225. https://doi.org/10.1016/j.compstruct.2017.12.036

Chen, C., Wang, X., Sui, L., Xing, F., Chen, X., & Zhou, Y. (2019). Influence of FRP thickness and confining effect on flexural performance of HB-strengthened RC beams. Composites Part B: Engineering, 161, 55–67. https://doi.org/10.1016/j.compositesb.2018.10.059

Codina, A., Barris, C., Jahani, Y., Baena, M., & Torres, L. (2023). Assessment of fib Bulletin 90 Design Provisions for Intermediate Crack Debonding in Flexural Concrete Elements Strengthened with Externally Bonded FRP. Polymers, 15(3). https://doi.org/10.3390/polym15030769

Consiglio Nazionalle delle Richerche (CNR). (2013). CNR-DT 200 R1/2013: Guide for the Design and Construction of Externally Guide for the Design and Construction of Externally Bonded FRP Systems for Strengthening Existing Structures (Issue January 2006). Consiglio Nazionalle delle Richerche (CNR).

fib Task Group 5.1. (2019). fib bulletin 90: Externally applied FRP reinforcement for concrete structures. Task Group 5.1 "Fibre-Reinforced Polymer Reinforcement for concrete structures".

Gao, L. (2020). Interfacial bonding characteristics and flexural performance of hybrid bonded FRP strengthened RC beams. Shandong University.

Gao, L., Wei, Q., Huang, Y., & Zhang, F. (2023). Influence of anchor design parameters on flexural performance of hybrid bonded-fiber reinforced polymer strengthened reinforced concrete beams. Structures, 48, 1029–1045. https://doi.org/10.1016/j.istruc.2023.01.025

Gao, L., Zhang, F., Liu, J., Lu, X., & Gao, H. (2019). Experimental and numerical study on the interfacial bonding characteristics of FRP-to-concrete joints with mechanical fastening. Construction and Building Materials, 199, 456–470. https://doi.org/10.1016/J.CONBUILDMAT.2018.12.033

Gao, X. H., Gao, L., & Zhang, F. (2023). A New Bond-Slip Model of Hybrid Bonded FRP-to-Concrete Joints. KSCE Journal of Civil Engineering, 27(1), 270–284. https://doi.org/10.1007/s12205-022-2286-4

Iovinella, I., Prota, A., & Mazzotti, C. (2013). Influence of surface roughness on the bond of FRP laminates to concrete. Construction and Building Materials, 40, 533–542. https://doi.org/10.1016/j.conbuildmat.2012.09.112

Mazzotti, C., Bilotta, A., Carloni, C., Ceroni, F., D'Antino, T., Nigro, E., & Pellegrino, C. (2016). Bond between EBR FRP and concrete. In RILEM State-of-the-Art Reports (Vol. 19, pp. 39–96). Springer Netherlands. https://doi.org/10.1007/978-94-017-7336-2_3

Teng, J. G., Smith, S. T., Yao, J., & Chen, J. F. (2003). Intermediate crack-induced debonding in RC beams and slabs. Construction and Building Materials, 17(6–7), 447–462. https://doi.org/10.1016/S0950-0618(03)00043-6

UNE-EN 12390-3. (2011). Testing hardened concrete - Part 3: Compressive strength of test specimens.

UNE-EN 12390-6. (2010). Testing hardened concrete - Part 6: Tensile splitting strength of test specimens.

UNE-EN ISO 15630-1. (2011). Steel for the Reinforcement and Prestressing of Concrete-Test Methods - Part 1: Reinforcing Bars, Wire Rod and Wire.

Wu, Y. F., Yan, J. H., Zhou, Y. W., & Xiao, Y. (2010). Ultimate strength of reinforced concrete beams retrofitted with hybrid bonded fiber-reinforced polymer. ACI Structural Journal, 107(4). https://doi.org/10.14359/51663818

Wu, Y.F., & Huang, Y. (2008). Hybrid Bonding of FRP to Reinforced Concrete Structures. Journal of Composites for Construction, 12(3). https://doi.org/10.1061/(asce)1090-0268(2008)12:3(266)

Wu, Y.F., & Liu, K. (2013). Characterization of Mechanically Enhanced FRP Bonding System. Journal of Composites for Construction, 17(1), 34–49. https://doi.org/10.1061/(ASCE)CC.1943-5614.0000302

Zhang, F., Gao, L., & Wei, Q. (2022). Theoretical and numerical bonding capacity model of FRP-to-concrete joints with mechanical fastening. Construction and Building Materials, 353. https://doi.org/10.1016/j.conbuildmat.2022.129066

Zhang, F., Gao, L., Wu, Y. F., & Liu, J. (2021). Flexural design of reinforced concrete structures strengthened with hybrid bonded FRP. Composite Structures, 269, 113996. https://doi.org/10.1016/J.COMPSTRUCT.2021.113996

Zhang, F., Gao, L., & Zhang, L. (2023). Numerical Simulation and Flexural Capacity of Hybrid-Bonded FRP Reinforced Concrete Beam. Arabian Journal for Science and Engineering, 48(10), 12845–12858. https://doi.org/10.1007/s13369-022-07587-7